ORIGINAL ARTICLE

Nr 2025;15 (1):66-70

Change in Polygon Shapes of Atrophic and Small Angular Fibers in Disuse Muscle Atrophy

Katsuhito Nagano

Department of Physical Therapy, Faculty of Health Sciences, Tsukuba International University, Ibaraki, Japan

CORRESPONDING AUTHOR:
Katsuhito Nagano
Department of Physical Therapy
Faculty of Health Sciences
Tsukuba International University
6-8-33 Manabe, Tsuchiura, Ibaraki
300-0051, Japan
E-mail: nagano@xg8.so-net.ne.jp

DOI:
10.32098/mltj.01.2025.08

LEVEL OF EVIDENCE: N/A (Animal study)

SUMMARY

Background. Muscle fiber (MF) cross-sectional area (CSA) and muscle strength are reduced in disuse muscle atrophy (DMA). However, whether approximate shapes of MF cross-section (AS-MFCS) are altered in DMA remains unknown. This study aimed to determine the AS-MFCS of atrophic MFs.

Methods. Eleven-week-old male Wistar rats were divided into control (CON) and sciatic nerve transection (SNT) groups before analysis of the soleus muscle.

Results. The CSA of atrophic fibers in the SNT group decreased to approximately 50% of that of MFs in the CON group. AS-MFCS in the CON and SNT groups were characterized by 5.6 and 5.5 vertices, respectively. The proportion of MFs with five or six angles accounted for 77% of the total fibers. The correlation between CSA and AS-MFCS was weak in both groups. The number of small angular fibers in the SNT group was significantly higher; however, CSA did not differ between the two groups.

Conclusions. These results revealed that CSA decreased at an early stage in the SNT group without major changes in the percentages of AS-MFCS. Moreover, the number of small angular fibers increased in the SNT group; however, the results suggest that effects on the number of vertices were minor at this stage.

KEY WORDS

Approximated polygon; atrophic fibers; disuse muscle atrophy; sciatic nerve transection; small angular fibers.

INTRODUCTION

Disuse muscle atrophy (DMA) is caused by physical inactivity, limb immobilization, prolonged bed rest, microgravity environment, and denervation, and results in reduced patients' activities of daily living and quality of life (1). Carnes *et al.* (2) have reported shapes of normal muscle fiber (MF) cross-sections (MFCSs) as elongated, cylindrical, and polygonal fibers. Torrejais MM *et al.* (3) have described them as polygonal, triangular, and circular, and Hojyo (4) have revealed them as tetragonal, pentagonal, hexagonal, and polygonal. However, these reports have not represented the methods used to determine approximate shapes of MFCS (AS-MFCS) or numerical data obtained for different shapes and have described the morphological features based only on investigators' subjective findings.

Since AS-MFCS are composed of linear sides, inflected sides with different angles, vertices with different angles, and rounded vertices, objective criteria for sides and vertices are required to determine the number of vertices in AS-MFCS analysis. Previously, we have established the criteria for vertices and edges to objectively determine AS-MFCS (Nagano's criteria for evaluation of MF shapes) and used the criteria to characterize AS-MFCS in untreated rats (5). Meanwhile, studies have shown decreases in muscle wet weight and MF cross-sectional area (CSA), changes in the ratio of fiber-type compositions, and increases in activation of proteolytic enzymes and degradation of muscle proteins in DMA (6, 7); however, changes in AS-MFCS have not been clarified. Moreover, small angular fibers occur in facioscapulohumeral muscular dystrophy, denervated myofibers, and after excessive exercise via electrical muscle stimulation. Small angular fibers have been reported to have small CSAs and sharp, angular vertices (8-11); however, their shapes have not been fully clarified.

This study aimed to characterize AS-MFCS of atrophic and small angular fibers in DMA based on Nagano's criteria for evaluating MF shapes and investigating their relationships with CSA.

MATERIALS AND METHODS

Grouping and intervention measures

This study was conducted in accordance with the "Act on Welfare and Management of Animals" of Japan, the "Guidelines for Proper Conduct of Animal Experiments" established by the Science Council of Japan, and the "International Guiding Principles for Biomedical Research Involving Animals" of the Council for International Organization of Medical Sciences and the International Council for Laboratory Animal Science. The study was approved by the Ethics Committee for Human Experiments of the Nittazuka Medical Welfare Center (registration number 26-5 - date of approval: April 16, 2024).

A total of ten 11-week-old male Wistar rats (body weight 307.8 ± 6.9 g) were divided into control (CON; 5 rats) and sciatic nerve transection (SNT; 5 rats) groups. The rats in the CON group were left untreated. To induce DMA, the rats in the SNT group were subjected to transection of the left sciatic nerve under deep anesthesia through intraperitoneal administration of a mixture anesthetic solution containing medetomidine hydrochloride (0.15 mg/kg), midazolam (2 mg/kg), and butorphanol tartrate (2.5 mg/kg). In both groups, each rat was maintained in a separate cage for 1 week with free access to water and food.

Quantitative morphology

A lethal dose of pentobarbital sodium (100 mg/kg) was administered to the rats, and the left soleus muscle was harvested as a muscle sample from each rat. The samples were cut transversely into two segments. Each segment was individually mounted on cork using the optimum cutting temperature compound (Sakura Finetek USA, Torrance, CA), and then the blocks were rapidly snap-frozen in isopentane cooled with dry ice–acetone and stored at -80 °C.

10-μm thick serial transverse cryosections were cut using a cryostat microtome (Leica Biosystems, Wetzlar, Germany) at -25 °C and mounted on silane-coated glass slides. The cryosections were air-dried for 60 minutes, fixed by immersion in cooled acetone at 4 °C, and subjected to hematoxylin–eosin staining according to the standard method (12).

Muscle tissue images were acquired using an optical microscope (Nikon Corporation, Tokyo, Japan), and 100 MFs per muscle (1000 MFs in total) in the central region of an image were selected to count the vertices and measure the CSA using the National Institutes of Health image processing software ImageJ 1.48u. Fibers that were clearly smaller than the surrounding MFs and had a CSA < 800 μm^2 were selected to count the vertices for small angular fibers. Nagano's criteria for evaluating MF shapes were used to identify edges and vertices of MFCSs (5).

Statistical analysis

IBM® SPSS Statistics 25 was used for statistical analysis. The data are shown in the form of mean ± standard deviation. Counts of vertices and MFCSAs were analyzed using the Shapiro-Wilk test for normality and Levene's test for variance. Spearman's rank correlation coefficient or Pearson product-moment correlation coefficient was used to analyze the correlation between the number of vertices and CSA. The Mann–Whitney U and Welch's t-tests were used for intergroup comparisons regarding the number of vertices and CSA, respectively. Bonferroni's multiple comparison test was used for intragroup comparisons of the proportions occupied by different approximated polygons and the MFCSAs of different approximated polygons. Differences with $p < 0.05$ were considered statistically significant.

RESULTS

Normal and atrophic MFs

In the CON group, the proportions of different AS-MFCS were 0.6% for triangles, 8.8% for tetragons, 40.2% for pentagons, 36.4% for hexagons, 12.0% for heptagons, and 2.0% for octagons (**figure 1A**). The proportion of pentagonal and hexagonal MFs combined was 76.6% of the total number of trigonal to octagonal MFs. Either of these two shapes accounted for a significantly greater proportion than triangles, tetragons, heptagons, or octagons ($p < 0.01$); however, there were no significant differences between the proportions of pentagons and hexagons (**figure 1A**).

In the SNT group, the proportions of different AS-MFCS were 0.6% for triangles, 10.2% for tetragons, 45.8% for pentagons, 31.8% for hexagons, 9.6% for heptagons, and 1.0% for octagons (**figure 1B**). Number of pentagonal and hexagonal MFs accounted for 77.6% of the total fibers in this group. Pentagons accounted for a significantly greater proportion than any other polygon ($p < 0.01$), while, in the CON group, a significant difference in the proportion was observed between the pentagons and hexagons (**figure 1B**). Based on the evaluation criteria of this study, AS-MFCS in

the CON and SNT groups had 5.6 ± 0.25 and 5.5 ± 0.12 vertices, respectively, showing that the means in the two groups did not differ significantly (**figure 1C**).
Compared to the CSA in the CON group (2,788.6 ± 198.3 μm²), the CSA in the SNT group was significantly smaller (1,403.0 ± 87.9 μm²) (**figure 1D**).
The correlation between the CSA and the number of vertices in the CON group was significant, but the correlation coefficient and coefficient of determination were low (rs = 0.159, R^2 = 0.024, p = 0.001) (**figure 1E**). These relationships in the SNT group were also not correlated (rs = 0.081, R^2 = 0.007, p = 0.068) (**figure 1F**).

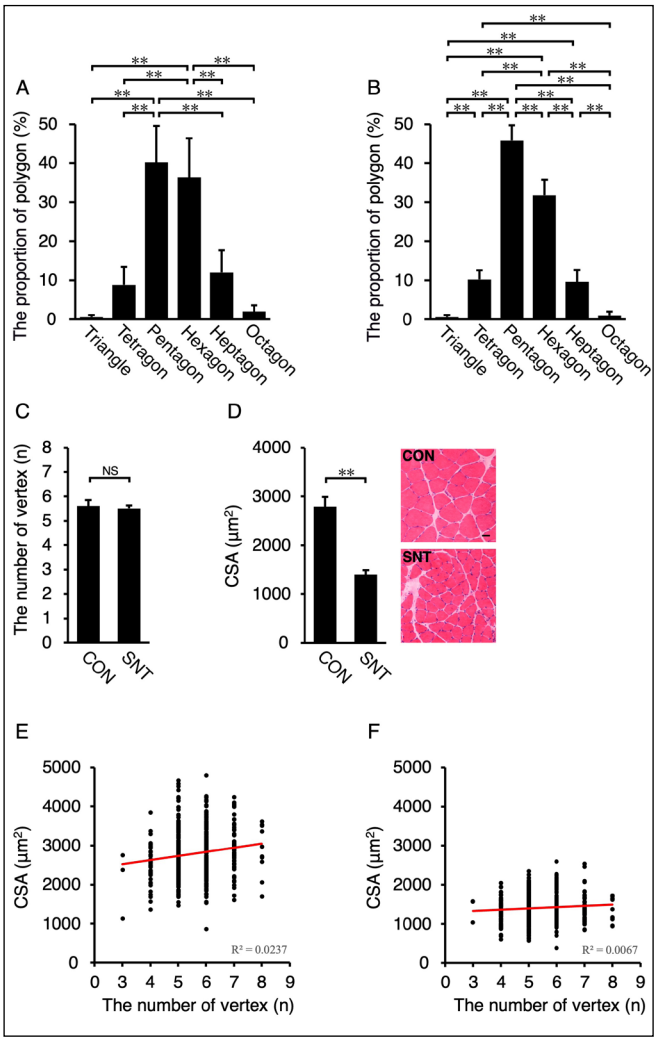

Figure 1. Comparison of approximate polygons, cross-sectional areas, and number of angles in atrophic muscle fibers.
A and E: CON group; B and F: SNT group; **P-value < 0.01; CON: Control; SNT: Sciatic nerve transection; CSA: Cross-sectional area; Scale bars: 50 μm; values are means ± standard deviation.

Small angular fibers

For small angular fibers in the CON group, proportions of different AS-MFCS were 0.0% for triangles, 16.7% for tetragons, 16.7% for pentagons, 36.4% for hexagons, 66.7% for heptagons, and 0.0% for octagons. Heptagons accounted for the greatest proportion (66.7%), which differed significantly from the proportion of triangles, hexagons, or octagons (p < 0.05) (**figure 2A**).
For small angular fibers in the SNT group, the proportions of different AS-MFCS were 0.0% for triangles, 17.2% for tetragons, 27.6% for pentagons, 34.5% for hexagons, 13.8% for heptagons, 13.4% for octagons, and 3.4% for nonagons. Hexagons accounted for the greatest proportion of small angular fibers in the SNT group, which differed significantly only from the proportion of triangles (p < 0.05) (**figure 2B**). Additionally, for all small angular fibers obtained from the CON and SNT groups, proportions of different AS-MFCS were 0.0% for triangles, 17.1% for tetragons, 25.7% for pentagons, 28.6% for hexagons, 22.0% for heptagons, 2.9% for octagons, and 2.9% for nonagons.
The angle count of the small angular fibers of CON was an average of 6.2 ± 1.2 angles and the angle count of the small angular fibers obtained from CON and SNT was an average of 5.7 ± 1.3 angles (n = 38) (**figure 2C**).
Small angular fibers were stained with no major differences from surrounding MFs, had a CSA significantly smaller than that of the surrounding MFs, and were observed in a scattered manner.
The number of small angular fibers in the SNT group (5.8 ± 2.4) was significantly greater than that in the CON group (1.2 ± 0.7) (p < 0.05) (**figure 2D**).
The CSA of small angular fibers was 257.4 ± 114.7 μm² in the CON group and 294.4 ± 77.5 μm² in the SNT group, with no significant differences between the two groups. The CSA of small angular fibers (n = 38) was 300.5 ± 121.1 μm² (**figure 2E**).
The correlation coefficients between the number of vertices and the CSA in the CON and SNT groups showed no significant relationships (r = 0.238, R^2 = 0.0057, p = 0.650) (r = 0.309, R^2 = 0.095, p = 0.103) (**figures 2F,G**).

DISCUSSION

In this study, AS-MFCS of atrophic and small angular fibers were measured based on Nagano's criteria for evaluating AS-MFCS. A mean number of vertices of 5 and a proportion of pentagons and hexagons of approximately 80% in the SNT group suggest that the atrophic fibers at this stage had mainly pentagonal and hexagonal CSs, like MFs in the CON group. The atrophic fibers in the SNT group had a

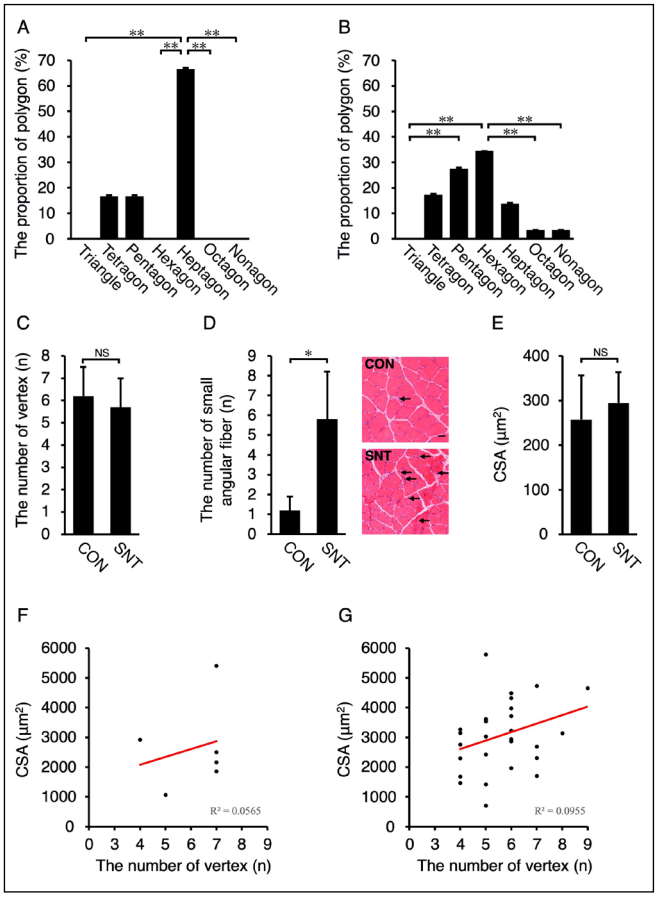

Figure 2. Comparison of approximate polygons, cross-sectional areas, and number of angles in small angular fibers.

A and F: CON group; B and G: SNT group; *P-value < 0.05; **P-value < 0.01; CON: Control; SNT: Sciatic nerve transection; CSA: Cross-sectional area; arrows indicate the small angular fibers; scale bars: 50 μm; values are means ± standard deviation.

markedly reduced CSA, which was approximately 50% of that of MFs in the CON group; however, the mean number of vertices did not differ between the two groups. The data revealed that the relationship between the number of vertices and the CSA was minimal in the early stage of MA, indicating that MFs undergo atrophy without appreciable shape changes.

However, in the CON group, the proportions of pentagons and hexagons differed from those of other polygons, with no differences between them. In contrast, the proportions also differed between pentagons and hexagons in the SNT group. This difference suggests the possibility that AS-MFCS converge to a pentagon or the number of vertices decreases overall with further progression of MA. Moreover, necrotic, apoptotic, and collagen fibers surrounding MFs have been reported to increase with the progression of MA, and the number of vertices may change as an effect of such histological changes (13).

Small angular fibers had a CSA approximately 1/10 and 1/5 as large as those of MFs in the CON group and atrophic fibers in the SNT group, respectively, and were observed as MFs smaller than other MFs in the vicinity. Approximately 70% of shapes of small angular fiber CS were accounted for by pentagons and hexagons, suggesting that pentagons and hexagons are their main shapes. Moreover, the proportions of hexagons and heptagons in small angular fibers tended to be more than those in MFs in the CON group and atrophic fibers in the SNT group, suggesting the possibility that the number of vertices increases further with the progression of MA.

Conventionally, small angular fibers have been defined ambiguously, and no strictly defined criteria for small angular fibers are available (14-17); however, based on the results of this study, a CSA of 1/10 or smaller than that of normal MFs, a CSA of 1/5 or smaller than that of atrophic MFs, and polygonal CSs with 4-9 vertices can constitute the criteria for small angular fibers.

Decrease of muscle mass and CAS in humans occurs with various causes including cancers (18), chronic obstructive pulmonary disease (19), chronic heart failure (20), sepsis (21), limb immobilization (22), muscular dystrophy (23), and spinal cord injury (24). Although the morphology of muscle fibers in these patients has not yet been elucidated, by clarifying the differences between the results of AF-MFCS for simple muscular atrophy obtained in this study and those of these diseases, it is possible to clarify the differentiation, severity, progression, and treatment effects of the disease.

Finally, it should be noted that the results of this study were obtained from the soleus muscles of 11-week-old rats. Therefore, these results may lack external validity due to differences in DMA models other than denervation model and soleus muscle, rat week-old, tissue fixation method, and progression of muscle atrophy. In the future, further studies are necessary to see whether similar results can be obtained in sarcopenia and myopathy, and changes in the number of vertices with further progression of DMA should also be addressed.

CONCLUSIONS

We found that atrophic fibers and small angular fibers in SNT have a high occupancy rate of pentagons and hexagons, and that the correlation between MFCSA and the number of angles is low in the early stages of muscle atrophy. It is clear that in the early stages of DMA, the CSA decreases with little change in the number of angles.

FUNDINGS
None.

DATA AVAILABILITY
Data are available under reasonable request to the corresponding author.

CONTRIBUTIONS
KN: animal experiments, data analysis and interpretation, writing – original draft, writing – review & editing.

CONFLICT OF INTERESTS
The author declares that he has no conflict of interests.

REFERENCES

1. Sayed RKA, Hibbert JE, Jorgenson KW, Hornberger TA. The Structural Adaptations That Mediate Disuse-Induced Atrophy of Skeletal Muscle. Cells. 2023;12(24):2811. doi: 10.3390/cells12242811.
2. Carnes ME, Pins GD. Skeletal Muscle Tissue Engineering: Biomaterials-Based Strategies for the Treatment of Volumetric Muscle Loss. Bioengineering (Basel). 2020;7(3):85. doi: 10.3390/bioengineering7030085.
3. Torrejais MM, Soares JC, Matheus SM, Cassel FD, Curi PR. Histochemical study of the extensor digitorum longus and soleus muscles in alcoholic rats. Anat Histol Embryol. 1999;28(5-6):367-73. doi: 10.1046/j.1439-0264.1999.00226.x.
4. Hojo H. Scanning electron microscopic observation of normal sekletal muscle. Showa Univ J Med Sci. 1980;41(3):233-40. doi: 10.1001/archneur.1973.00490220055008.
5. Nagano K. Quantitative analysis of approximate shapes in a myofiber cross-section and their relationship with myofiber cross-sectional area. J Phys Ther Sci. 2021;33:931-34. doi: 10.1589/jpts.33.931.
6. Riley DA, Slocum GR, Bain JL, Sedlak FR, Sowa TE, Mellender JW. Rat hindlimb unloading: soleus histochemistry, ultrastructure, and electromyography. J Appl Physiol. 1990;69(1):58-66. doi: 10.1152/jappl.1990.69.1.58.
7. Zhang P, Chen X, Fan M. Signaling mechanisms involved in disuse muscle atrophy. Med Hypotheses. 2007;69(2):310-21. doi: 10.1016/j.mehy.2006.11.043.
8. Lin MY, Nonaka I. Facioscapulohumeral muscular dystrophy: muscle fiber type analysis with particular reference to small angular fibers. Brain Dev. 1991;13(5):331-8. doi: 10.1016/s0387-7604(12)80128-8.
9. Scelsi R, Marchetti C, Poggi P. Histochemical and ultrastructural aspects of m. vastus lateralis in sedentary old people (age 65-89 years). Acta Neuropathol. 1980;51(2):99-105. doi: 10.1007/BF00690450.
10. Lexell J, Taylor CC. Variability in muscle fibre areas in whole human quadriceps muscle: effects of increasing age. J Anat. 1991;174:239-49.
11. Song Y, Forsgren S, Yu J, Lorentzon R, Stål PS. Effects on contralateral muscles after unilateral electrical muscle stimulation and exercise. PLoS One. 2012;7(12):e52230. doi: 10.1371/journal.pone.0052230.
12. Wang C, Yue F, Kuang S. Muscle Histology Characterization Using H&E Staining and Muscle Fiber Type Classification Using Immunofluorescence Staining. Bio Protoc. 2017;7(10):e2279. doi: 10.21769/BioProtoc.2279.
13. Hu NF, Chang H, Du B, et al. Tetramethylpyrazine ameliorated disuse-induced gastrocnemius muscle atrophy in hindlimb unloading rats through suppression of Ca2+/ROS-mediated apoptosis. Appl Physiol Nutr Metab. 2017;42(2):117-27. doi: 10.1139/apnm-2016-0363.
14. Doppler K, Mittelbronn M, Bornemann A. Myogenesis in human denervated muscle biopsies. Muscle Nerve. 2008;37(1):79-83. doi: 10.1002/mus.20902.
15. Kojima S, Takagi A, Ida M, Shiozawa R. Muscle pathology in polymyalgia rheumatica: histochemical and immunohistochemical study. Jpn J Med. 1991;30(6):516-23. doi: 10.2169/internalmedicine1962.30.516.
16. Mosole S, Carraro U, Kern H, Loefler S, Zampieri S. Use it or Lose It: Tonic Activity of Slow Motoneurons Promotes Their Survival and Preferentially Increases Slow Fiber-Type Groupings in Muscles of Old Lifelong Recreational Sportsmen. Eur J Transl Myol. 2016;26(4):5972. doi: 10.4081/ejtm.2016.5972.
17. Yogev Y, Perez Y, Noyman I, et al. Progressive hereditary spastic paraplegia caused by a homozygous KY mutation. Eur J Hum Genet. 2017;25(8):966-72. doi: 10.1038/ejhg.2017.85
18. Zhang Y, Wang J, Wang X, et al. The autophagic-lysosomal and ubiquitin proteasome systems are simultaneously activated in the skeletal muscle of gastric cancer patients with cachexia. Am J Clin Nutr. 2020;111(3):570-9. doi: 10.1093/ajcn/nqz347.
19. Kritikaki E, Terzis G, Soundararajan M, Vogiatzis I, Simoes DCM. Expression of intramuscular extracellular matrix proteins in vastus lateralis muscle fibres between atrophic and non-atrophic COPD. ERJ Open Res. 2024;10(3):00857-2023. doi: 10.1183/23120541.00857-2023.
20. Emami A, Saitoh M, Valentova M, et al. Comparison of sarcopenia and cachexia in men with chronic heart failure: results from the Studies Investigating Co-morbidities Aggravating Heart Failure (SICA-HF). Eur J Heart Fail. 2018;20(11):1580-7. doi: 10.1002/ejhf.1304.
21. Chun SY, Cho YS, Kim HB. Association between reduced muscle mass and poor prognosis of biliary sepsis. Sci Rep. 2024;14(1):1857. doi: 10.1038/s41598-024-52502-9.
22. Yoshiko A, Yamauchi K, Kato T, et al. Effects of post-fracture non-weight-bearing immobilization on muscle atrophy, intramuscular and intermuscular adipose tissues in the thigh and calf. Skeletal Radiol. 2018;47(11):1541-9. doi: 10.1007/s00256-018-2985-6.
23. Liu M, Chino N, Ishihara T. Muscle damage progression in Duchenne muscular dystrophy evaluated by a new quantitative computed tomography method. Arch Phys Med Rehabil. 1993;74(5):507-14. doi: 10.1016/0003-9993(93)90115-q.
24. Castro MJ, Apple DF Jr, Staron RS, Campos GE, Dudley GA. Influence of complete spinal cord injury on skeletal muscle within 6 mo of injury. J Appl Physiol (1985). 1999;86(1):350-8. doi: 10.1152/jappl.1999.86.1.350.